Modeling a Fe-Ga Energy Harvester Fitted with Magnetic Closure Using 3D Magneto-Mechanical Finite Element Model

U. Ahmed[a]*, U. Aydin[a, b], M. Zucca[c], S. Palumbo[c, d], R. Kouhia[e], P. Rasilo[a]

[a] *Tampere University, Electrical Engineering, P.O. Box 692, FI-33720, Tampere (Hervanta campus), Finland*
[b] *Aalto University, Department of Electrical Engineering and Automation, P.O. Box 15500, FI-00076, Espoo, Finland*
[c] *Istituto Nazionale di Ricerca Metrologica, INRIM, Strada delle Cacce 91, Torino, Italy*
[d] *Politecnico di Torino, Dipartimento di Elettronica e Telecomunicazioni, Corso Duca degli Abruzzi 24, Torino, Italy*
[e] *Tampere University, Civil Engineering, P.O. Box 600, 33014 Tampere University (Hervanta campus), Finland*

ARTICLE INFO

Keywords:
Energy harvesting
Finite element analysis
Magneto-elasticity
Helmholtz free energy
Magnetostrictive devices

ABSTRACT

This paper presents the implementation of magneto-mechanical constitutive law utilizing thermodynamic approach in a 3D finite element solver using COMSOL Multiphysics software. The analytical expression for the magnetic field strength and stress is derived from the constitutive model utilizing magnetic flux density and mechanical strain as state variables. The constitutive model is successfully implemented in commercially available software COMSOL. This implementation allows 3D analysis of an energy harvester device efficiently and accurately. A prototype concept device is developed to validate the model and its implementation. The device is tested under uniaxial compressive loading by varying the preload, dynamic load and magnetic bias. The model is validated by comparing the simulated and experimental results. The comparison shows that the model can reasonably predict the optimal value of the preload and magnetic bias yielding maximum power and is able to follow the measurement trends. This model can be used as a suitable tool to analyze the behavior of the concept energy harvesters and determine the optimal design parameters.

1. Introduction

Magneto-mechanical energy harvesters based on giant magnetostrictive materials (GMMs) allow conversion of ambient vibration energy from moving parts of machines, bridges and rail tracks etc. into electrical energy to power-up small-scale sensors and microelectronic systems. This enables an autonomous and battery free solution for wireless sensor nodes suitable in various applications including structural condition monitoring and biomedical applications. The GMMs can be utilized as transducers for active vibration control sensors. Among GMMs, galfenol exhibits strong magneto-mechanical coupling, low hysteresis losses, and high tensile strength (~500 MPa) as compared to Terfenol-D, making it a suitable candidate to be incorporated as an active material for the energy harvester. Terfenol-D is brittle in nature having low tensile strength (28–40 MPa) with poor machinability whereas galfenol can be welded and machined easily, thus providing more practical options to be utilized as an active material. A comparison among the characteristics of Terfenol-D and galfenol is presented in [1].

The design process of an energy harvester requires knowledge about the characteristics of the active material, the external operating conditions (magnetic bias, frequency and amplitude of mechanical vibrations) as well as the device design (geometry). Numerous studies have been carried out related to modeling and design of magnetostrictive energy harvesters [2], [3]. During last decade, the focus has shifted towards optimizing the device design and determining the optimal operating conditions to maximize the potential of the harvesters [3–6]. Modeling tools are required to analyze the coupled magneto-mechanical effects in ferromagnetic materials to determine efficient device design and optimal operating conditions for the energy harvester. Various models have been developed to study the effect of design parameters [5–8], but there is a lack of knowledge related to the influence of the several design parameters yielding maximum output power, which include the geometry of the device, applied magnetic bias, external loading and magnetic closure circuit. Moreover, there is no generic model to fully analyze the behavior of the energy harvester or to suggest suitable operating conditions and design parameters.

The proposed paper utilizes thermodynamic magneto-mechanical constitutive laws developed in [9] to be implemented in a 3D finite element (FE) model using COMSOL Multiphysics software. The model is validated by comparing the measurement results obtained from the prototype energy harvester concept device developed in [5]. The aim of this paper is to implement the model presented in [9] for the 3D analysis of an energy harvester device that includes a magnetic flux closure constructed with soft magnetic material. The results are analyzed to determine the influence of the design parameters (magnetic bias and preload) on the device performance.

2. Experimental setup and working principle

2.1. Material characterization

The experimental setup is presented in two parts. In the first setup, the characterization of the material is performed for

*Corresponding author: Umair Ahmed
Email address: umair.ahmed@tuni.fi

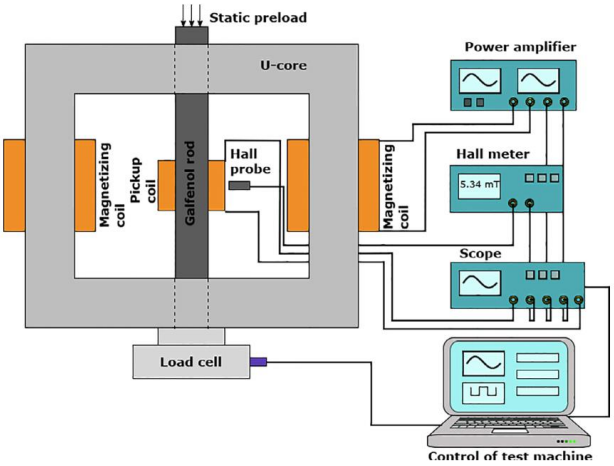

Fig. 1. Schematic diagram for the characterization of the material.

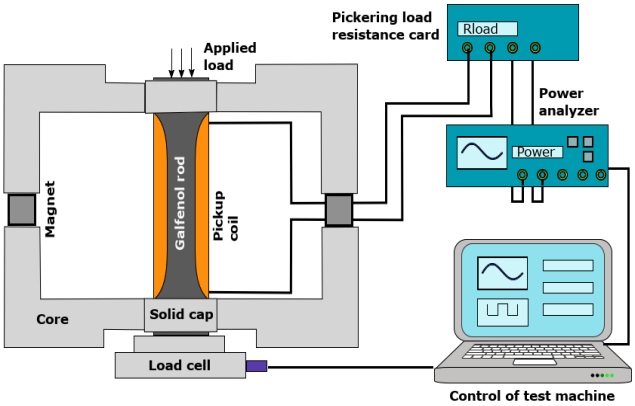

Fig. 2. Schematic diagram of the complete energy harvester setup and the internal structure of machined galfenol rod (sliced diagram).

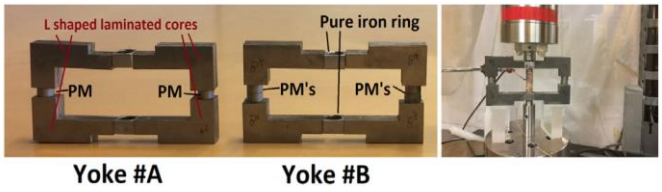

Fig. 3. The actual setup for the energy harvester (right), magnetic closure circuit with 2 magnets (Yoke #A) and 4 magnets (Yoke #B) on both sides.

the identification of the constitutive laws describing the magneto-elastic behavior. A cylindrical rod of galfenol ($Fe_{81.6}Ga_{18.4}$) is used as the active material for the prototype energy harvesting concept device. The overall dimensions of the rod are 60 mm in length with the diameter of 12 mm [9]. The magnetization (B–H) and magnetostriction curves were obtained under various static axial compressive prestress (preload) σ values ranging from 0 to 80 MPa. The complete setup for the material characterization is presented in Fig. 1 where the galfenol rod is magnetized with the help of two coils and a U-shaped core. The Hall probe measures the magnetic field strength H near the middle part of the sample. The magnetic flux density B is obtained by integrating the induced voltage from the pickup coil wound around the sample.

2.2. Energy harvester

The second setup is related to the energy harvester consisting of a galfenol rod as an active material which is magnetized with the help of permanent magnets and four L-shaped cores. The schematic diagram of the prototype harvester concept device is presented in Fig. 2. The galfenol rod is first machined to accommodate the pickup coil consisting of 2000 turns with the wire diameter of 0.2 mm as shown in Fig. 2. After machining the sample, the diameter of the sample is reduced to 6 mm for the length of 48 mm. The actual experimental setup is shown in Fig. 3. A constant magnetic bias is applied using NdFeB magnets having a remanence flux density of B_r = 1.1 T and coercive field strength of H_c = 955 kA/m with physical dimensions of 6 mm in thickness and 12 mm in diameter.

Two different cases were studied during experimentation indicated as Yoke#A and Yoke#B in Fig. 3. The case Yoke#A consists of one magnet on each column whereas Yoke#B has two magnets on both columns. The length of the columns from the L-shaped core is reduced to accommodate the magnets so that the overall length of the magnetic circuit remains the same.

For the energy harvester setup, the galfenol rod is first subjected to static compressive preload σ followed by a sinusoidal dynamic compressive load with amplitude $\Delta\sigma$ and frequency of 100 Hz. The voltage is induced into the pickup coil due to applied dynamic load ($\Delta\sigma$) because of inverse magnetostrictive effect and Faraday's law. The output power is measured using 160 Ω load resistance for preload σ = 20–80 MPa keeping the dynamic load and vibration frequency constant. The maximum power is obtained as a function of magnetic bias and preload. In this study, we test the ability of the model in reproducing the effect of magnetic bias, preload and dynamic load on the harvester.

3. Models

3.1. Constitutive model

The derivation of coupled magneto-mechanical constitutive laws for the actuator material in an energy harvester using a thermodynamic approach is presented in [9]. The approach is based on deriving the Helmholtz free energy density $\psi(\boldsymbol{B}, \boldsymbol{\varepsilon})$ as a function of magnetic flux density vector $\boldsymbol{B}$ and strain tensor $\boldsymbol{\varepsilon}$. Assuming the actuator material to be isotropic, the state variables $\boldsymbol{B}$ and $\boldsymbol{\varepsilon}$ are written in terms of six scalar invariants. The analytical expressions for the invariants can be found from [9]. The Helmholtz free energy density describing coupled magneto-mechanical behavior in the actuator material is written as

$$\psi = \frac{1}{2}\lambda I_1^2 + \mu I_2 + \sum_{i=1}^{n_\alpha} \alpha_i I_4^i + \sum_{i=1}^{n_\beta} \beta_i I_5^i + \sum_{i=1}^{n_\gamma} \gamma_i I_6^i \,, \qquad (1)$$

where λ and μ are the Lamé parameters obtained from Young's modulus and Poisson's ratio, and the fitting parameters α_i, β_i and γ_i are polynomial coefficients fitted

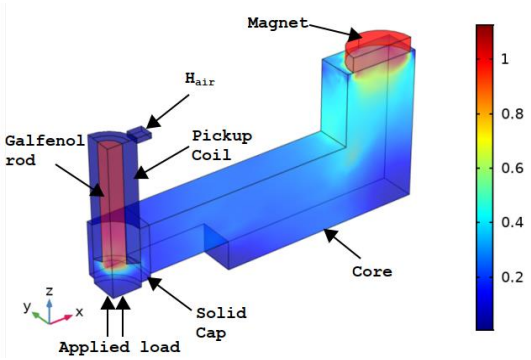

Fig. 4. The geometry of the model implemented in COMSOL for 3D FE simulation. Legend bar denotes magnetic flux density norm (T).

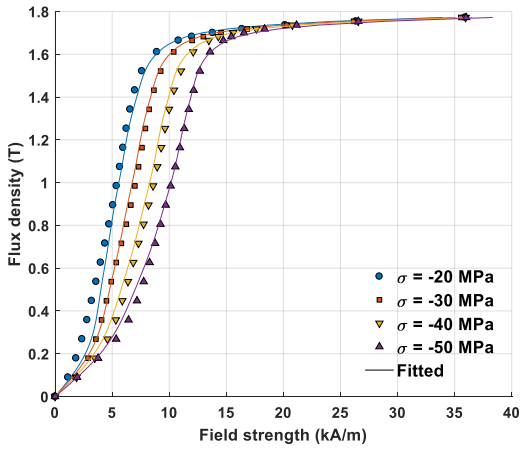

Fig. 5. Measured and fitted magnetization curves under different values of static compressive stress (σ).

against the *B*–*H* curves obtained from the characterization of the material discussed in Section 2.1. The invariants I_1 and I_2 describe pure mechanical behavior, I_4 describe magnetic behavior and I_5 and I_6 describe magneto-elastic behavior. The invariant I_3 is not utilized considering linear elastic behavior of the material. The constitutive equations for the magnetic field strength $\boldsymbol{H}$ and the Cauchy stress tensor $\boldsymbol{\sigma}$ are thus derived by computing the partial derivatives of ψ with respect to $\boldsymbol{B}$ and $\boldsymbol{\varepsilon}$

$$\boldsymbol{H}(\boldsymbol{B},\boldsymbol{\varepsilon}) = \left(\frac{\partial \psi}{\partial \boldsymbol{B}}\right)^{\mathrm{T}} \text{ and } \boldsymbol{\sigma}(\boldsymbol{B},\boldsymbol{\varepsilon}) = \frac{\partial \psi}{\partial \boldsymbol{\varepsilon}} \tag{2}$$

where T denotes the transpose of a vector. The constitutive equations are symbolically derived in MATLAB, and their free parameters α_i, β_i and γ_i are fitted to the measurement data from the characterization of the material. The constitutive model allows analytical calculation of $\boldsymbol{H}$ and $\boldsymbol{\sigma}$ as a function of $\boldsymbol{B}$ and $\boldsymbol{\varepsilon}$.

3.2. Finite element model

The constitutive equations developed in section 3.1 are implemented in a 3D FE solver in COMSOL. The 3D magneto-mechanical FE simulation is carried out for 1/8$^{\text{th}}$ of the geometry presented in Fig. 4. The magnetic field strength H_{air} is computed near the middle part of the sample and mechanical stress is applied at the bottom of the sample indicated by arrows pointing in Fig. 4. The magnetic field interface is added which solves for the Maxwell's equations to compute the electromagnetic fields. The solid mechanics interface is added for the active material that solves the mechanical balance equations. The material model (2) based on ψ is implemented by overriding the electromagnetic and mechanical constitutive models. The magneto-mechanical FE model is then based on solving the mechanical balance equations together with the combination of Faraday's and Ampere's laws:

$$\nabla \cdot \boldsymbol{\sigma}(\boldsymbol{B},\boldsymbol{\varepsilon}) = 0\,, \tag{3}$$

$$\nabla \times \boldsymbol{H}(\boldsymbol{B},\boldsymbol{\varepsilon}) + \kappa \frac{\partial \boldsymbol{A}}{\partial t} = 0\,, \tag{4}$$

where κ is the electrical conductivity and $\boldsymbol{A}$ is the magnetic vector potential. The flux density and strain are obtained as $\boldsymbol{B} = \nabla \times \boldsymbol{A}$ and $\boldsymbol{\varepsilon} = (\nabla \boldsymbol{u} + (\nabla \boldsymbol{u})^{\mathrm{T}})/2$, where $\boldsymbol{u}$ is the displacement vector used as the field variable. The partial differential equations (3) and (4) are coupled through the constitutive law (1) and (2). In other regions only the electromagnetic problem is solved as

$$\nabla \times \nu \nabla \times \boldsymbol{A} + \kappa \frac{\partial \boldsymbol{A}}{\partial t} = \boldsymbol{J}_{\mathrm{s}} + \nabla \times \boldsymbol{H}_{\mathrm{c}}\,, \tag{5}$$

where $\boldsymbol{J}_{\mathrm{s}} = (Ni_{\mathrm{coil}}/S_{\mathrm{coil}})\boldsymbol{e}_{\theta}$ is the circumferential source current in the pickup coil with N turns, cross-sectional area S_{coil} and current i_{coil} (nonzero only in the coil), κ is the electrical conductivity of the parts modeled as solid conductors (nonzero only in the permanent magnets and caps) shown in Fig. 4. $\boldsymbol{H}_{\mathrm{c}}$ is coercive field of the permanent magnets (nonzero only in the magnets). The electric circuit interface is added to compute the current and voltage across the load resistance R_{load}. The coil internal resistance (R_{coil} = 32.6 Ω) is given as a parameter and the coil current i_{coil} is computed from the partial derivation of the vector potential $\boldsymbol{A}$ in the coil as

$$\begin{aligned} \phi &= N \oint_{\Omega \mathrm{coil}} \boldsymbol{A} \cdot d\boldsymbol{l} \\ \frac{\partial \phi}{\partial t} &= -(R_{\mathrm{coil}} + R_{\mathrm{load}})\, i_{\mathrm{coil}} \end{aligned}\,, \tag{6}$$

where Ω_{coil} is the domain where line integral is computed and ϕ is the total flux linkage of the coil with N turns. The tangential components of the magnetic vector potential $\boldsymbol{A}$ are fixed to zero at the outer boundaries and the displacements perpendicular to the x = 0, y = 0 and z = 0 planes are fixed to zero as seen from Fig. 4. The Backward-Euler method is used for time integration of the Ampere's law and the resulting discretized non-linear algebraic equation system is solved using the Newton-Raphson iteration.

4. Results

The magnetization curves (*B*–*H*) obtained during the characterization of the material in Section 2.1 are fitted to the analytical expression (1). The result of the fitting to the

measured B–H curves at preload values ranging from 20 to 50 MPa is presented in Fig. 5. Owing to very low hysteresis losses discussed in [2] and [5], the fitting is done using a single valued B–H curve obtained by averaging the major hysteresis loop in the H-direction. The values of the fitting parameters α_i, β_i and γ_i for η_α = 11, η_β = 1 and η_γ = 2 are presented in the Table. 1.

Table 1. Coefficients of the fitting parameters

Parameter	Value (J/m^3)	Parameter	Value (J/m^3)
α_1	6.89×10^3	α_8	-1.63×10^4
α_2	-1.72×10^4	α_9	3.80×10^3
α_3	4.51×10^4	α_{10}	-509.9
α_4	-8.08×10^4	α_{11}	29.89
α_5	9.79×10^4	β_1	-1.76×10^6
α_6	-8.03×10^4	γ_1	8.13×10^9
α_7	4.44×10^4	γ_2	-1.76×10^5

For the energy harvester setup discussed in Section 2.2, 3D FE simulations are carried out changing the operating conditions (magnetic bias and preload) to validate the model and its implementation in COMSOL. As discussed earlier, the output power of the energy harvester is governed by the choice of load resistance and available mechanical excitation. Quite often, we do not have control over the load or the amplitude or frequency of mechanical vibration (ambient vibrational sources). Therefore, for the sake of comparison with the measured results in [5], all simulations are done keeping constant load resistance (R_{load} = 160 Ω), peak amplitude of vibrations ($\Delta\sigma$ = 8 MPa) and the excitation frequency of 100 Hz.

The simulated results are computed by varying the preload (σ) ranging from 20–80 MPa for both the cases Yoke#A and Yoke#B. The applied preload changes the magnetic bias in the magnetic circuit for both cases. The influence of changing preload and magnetic bias on the average output power is presented in Fig. 6. Since we are mainly interested in determining the optimal operating conditions yielding maximum power, the simulation is done for the specific preload range (20–80). The maximum power in both simulated and measured results is obtained at 45 MPa for Yoke#A and 55 MPa for Yoke#B. The comparison among the mean values of the measured and simulated magnetic field H_{air} computed near the middle part of sample for Yoke#A and Yoke#B and average power for Yoke#A is presented in Fig. 7 (a) and (b), respectively. The influence of preload over simulated magnetic flux density inside the bar (B_{bar}) and average power for Yoke#B is presented in Fig. 7 (c). The results from Fig 7(c) indicate that the permeability of the material decreases by increasing preload and the maximum power is obtained at 55 MPa. The results from Fig. 6 and Fig. 7 illustrate that there exists an optimal value of preload and magnetic bias for each specific case (Yoke#A and Yoke#B) resulting in maximum output power. In addition, the simulated results are in reasonable agreement with the measurements for the range of 20–50 MPa for which the fitting has been done. The difference

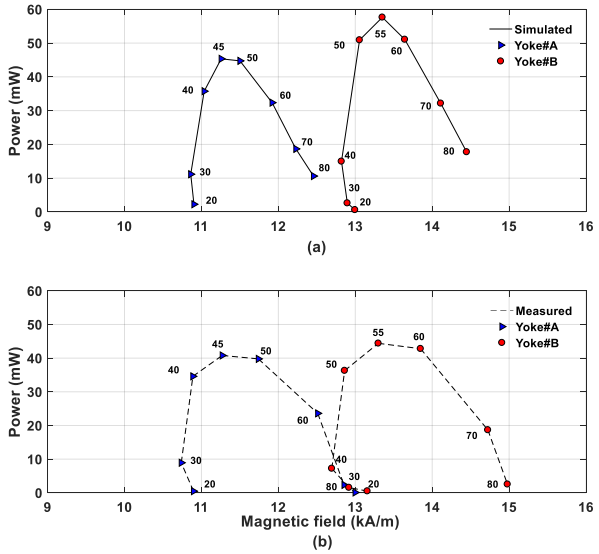

Fig. 6. Comparison among simulated (a) and measured (b) output power using R_{load} of 160 Ω, dynamic load of 8 MPa for different preload values in two different cases (Yoke#A and Yoke#B). The vibration freqeuncy is 100 Hz.

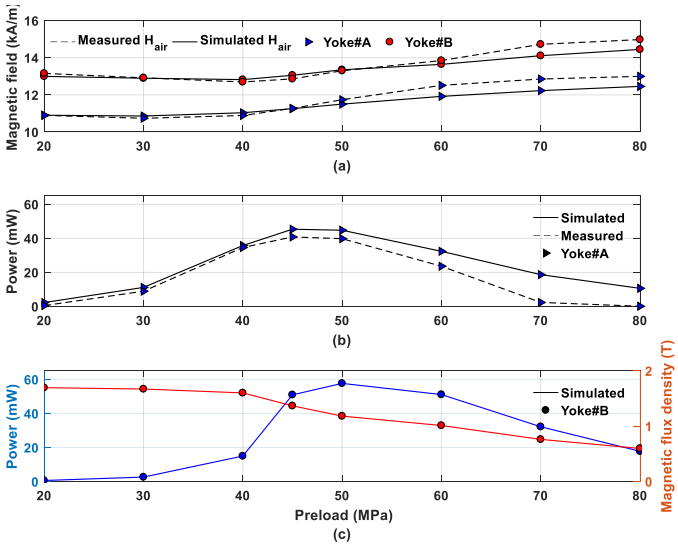

Fig. 7. Comparison among measured and simulated magnetic field H_{air} (a) and average powers with respect to changing preload (b). The simulated results of magnetic flux density B_{bar} and average power with respect to changing preload (c).

among measured and simulated results increases for higher stress values which is evident from Fig. 6 and Fig 7.

This difference is because, the model overestimates the relative permeability of the material for the range of 60–80 MPa. This causes smaller simulated magnetic field in the air (H_{air}) as compared to measured one. The overestimation of the relative permeability of the material results in larger values of the simulated power. Moreover, the simulation does not account for the small air gaps due to manufacturing tolerances between the solid cap, core and bar, which decreases the reluctance of the magnetic circuit causing an increase in simulated power. Furthermore, the experimental results are

affected by a measurement uncertainty, due to the accuracy of the field meter and due to the measurement repeatability [5] being anyway limited to few percent. Thus, the comparison among measured and simulated results should be made taking into account the uncertainty of the experimental results and model limitations.

5. Discussion and conclusion

This paper presents successful implementation of a magneto-mechanical constitutive law utilizing thermodynamic approach into a 3D FE model using commercially available COMSOL software. The model is validated by comparing the simulated and measured results for an energy harvester setup. The simulated results indicate that the model can reasonably predict the output power for the fitting range presented in Fig. 5. In addition, the model could also predict the optimal preload value and magnetic bias yielding maximum power.

Although the model reasonably describes the behavior of the studies devices, differences between the modeled and measured results are observed under some cases, particularly where the pre-load stress is above 60 MPa. These differences are associated with the measurement uncertainties and limitations of the model. In particular, the measurements were found to be sensitive to the vertical loading system of machine. These effects cause small discrepancies in the measurements. Moreover, the model can reasonably follow the trend of the measured results but is unable to accurately predict the results outside the range of data used for the fitting.

Furthermore, it was observed that tuning the simulated magnetic field H_{air} to the measured field improves the accuracy of results. The simulated results validate that, indeed there exists an optimal value of preload and magnetic bias resulting in maximum power. Tuning the external operating conditions (magnetic bias, preload, load resistance frequency and amplitude of vibrations) is important for the design and application prospective for the energy harvester. The proposed modeling approach can be applied to analyze a magneto-mechanical energy harvester and determine the optimal design characteristics and operating conditions.

References

[1] Berbyuk, V., 2013, April. Vibration energy harvesting using Galfenol-based transducer. In *Active and Passive Smart Structures and Integrated Systems 2013* (Vol. 8688, p. 86881F). International Society for Optics and Photonics.

[2] Clemente, C.S., Mahgoub, A., Davino, D. and Visone, C., 2017. Multiphysics circuit of a magnetostrictive energy harvesting device. *Journal of Intelligent Material Systems and Structures*, *28*(17), pp.2317–2330.

[3] Davino, D., Krejčí, P. and Visone, C., 2013. Fully coupled modeling of magneto-mechanical hysteresis through thermodynamic compatibility. *Smart Materials and Structures*, *22*(9), p.095009.

[4] Rezaeealam, B., 2012. Finite element analysis of magnetostrictive vibration energy harvester. *COMPEL-The international journal for computation and mathematics in electrical and electronic engineering*, *31*(6), pp.1757–1773.

[5] Palumbo, S., Rasilo, P. and Zucca, M., 2019. Experimental investigation on a Fe-Ga close yoke vibrational harvester by matching magnetic and mechanical biases. *Journal of Magnetism and Magnetic Materials*, *469*, pp.354–363.

[6] Atulasimha, J. and Flatau, A.B., 2011. A review of magnetostrictive iron–gallium alloys. *Smart Materials and Structures*, *20*(4), p.043001.

[7] Evans, P.G. and Dapino, M.J., 2010. Dynamic model for 3-D magnetostrictive transducers. *IEEE Transactions on Magnetics*, *47*(1), pp.221-230.

[8] Chakrabarti, S. and Dapino, M.J., 2012. Coupled axisymmetric finite element model of a hydraulically amplified magnetostrictive actuator for active powertrain mounts. *Finite Elements in Analysis and Design*, *60*, pp.25–34.

[9] Ahmed, U., Jeronen, J., Zucca, M., Palumbo, S. and Rasilo, P., 2019. Finite element analysis of magnetostrictive energy harvesting concept device utilizing thermodynamic magneto-mechanical model. *Journal of Magnetism and Magnetic Materials*, *486*, p.165275.

[10] Fonteyn, K., Belahcen, A., Kouhia, R., Rasilo, P. and Arkkio, A., 2010. FEM for directly coupled magneto-mechanical phenomena in electrical machines. *IEEE Transactions on Magnetics*, *46*(8),pp.2923–2926.